

# Entangled two-photon absorption with Brownian-oscillator fluctuations

Cite as: J. Chem. Phys. 156, 074303 (2022); doi: 10.1063/5.0082500

Submitted: 15 December 2021 • Accepted: 26 January 2022 •

Published Online: 15 February 2022



View Online



Export Citation



CrossMark

Feng Chen<sup>a)</sup>  and Shaul Mukamel<sup>b)</sup> 

## AFFILIATIONS

Department of Chemistry and Department of Physics and Astronomy, University of California, Irvine, California 92697, USA

<sup>a)</sup>Electronic mail: [chenf7@uci.edu](mailto:chenf7@uci.edu)

<sup>b)</sup>Author to whom correspondence should be addressed: [smukamel@uci.edu](mailto:smukamel@uci.edu)

## ABSTRACT

We theoretically investigate the two-photon absorption signals of a three-band ( $g, e, f$ ) system diagonally coupled to an over-damped Brownian oscillator bath, which induces random Gaussian modulations of energy levels with an arbitrary degree of correlation. For fast modulation, extra  $2\omega_{eg}$  and  $2\omega_{fe}$  peaks may obscure the  $g-f$  transitions in the classical two-photon absorption (CTPA) spectra for nearly resonant  $e$  states. These peaks arise from one-photon resonant  $g-e$  or  $e-f$  transitions. In the slow modulation limit, these peaks vanish because of the short tails of the Gaussian line shape. CTPA strongly depends on the correlations between energy fluctuations. In entangled two-photon absorption, the extra peaks are eliminated because of the broad one-photon but narrow two-photon spectrum of the twin photons. The variation of the coherences between  $f$  states with the correlation between energy fluctuations is explored.

Published under an exclusive license by AIP Publishing. <https://doi.org/10.1063/5.0082500>

## I. INTRODUCTION

In two-photon absorption (TPA), the molecule absorbs two photons and is promoted from the ground state  $g$  to a final excited state  $f$  via an intermediate state  $e$  [see Fig. 1(a)]. Since its discovery in the 1930s, TPA has been employed in spectroscopy, optical data storage, and fluorescence imaging.<sup>1</sup> Stimulated by the creation of quantum states of light, efforts have been made to explore the non-linear spectroscopy with time-energy entangled photons.<sup>2-4</sup> Entangled TPA (ETPA) contains notable advantages compared to classical TPA (CTPA), including the linear rather than quadratic scaling with the field intensity,<sup>5-7</sup> accessing classically disallowed excitations,<sup>8,9</sup> and the control of transition pathways.<sup>10,11</sup> Some experiments<sup>12-14</sup> have reported that nearly 10 orders of magnitude lower incident photon flux is required for ETPA compared to CTPA, thus reducing the damage in the imaging of biological samples. However, recent experiments<sup>15,16</sup> and theoretical calculations<sup>17,18</sup> cast doubt on the magnitude of this enhancement and raise the question of whether the signals observed in previous experiments were caused by one-photon mechanisms.<sup>19</sup>

Most theoretical simulations of TPA signals in atomic or molecular systems are so far based on the wavefunction treatment that only includes lifetime broadening,<sup>20</sup> density matrix

treatment that includes homogeneous broadening,<sup>17</sup> or convolution with a Gaussian distribution to account for inhomogeneous broadening.<sup>21,22</sup>

Here, we simulate the TPA signals of a multi-level system diagonally coupled to an over-damped Brownian oscillator bath,<sup>23</sup> which causes Gaussian fluctuations of the energy levels and is a realistic model for the surrounding environment in condensed phases. The intermediate state  $e$  in a TPA process is ideally taken to be far off-resonant (i.e., virtual), but strong enhancement of TPA has been observed for resonant intermediate states.<sup>22,24,25</sup> We find that when  $\omega_{fg} \approx 2\omega_{eg}$ , extra peaks appear in CTPA signals in the fast modulation limit, which may interfere with the  $\omega_{fg}$  peaks. The extra peaks originate from one-photon resonant  $g-e$  or  $e-f$  transitions and vanish in the slow modulation limit because of the short tails of Gaussian line shapes. CTPA signals also depend on the correlation between fluctuations:  $2\omega_{eg}$  peaks are weakened,  $2\omega_{fe}$  peaks are strengthened and sharpened, and  $\omega_{fg}$  peaks are shifted as the correlation between  $\omega_{eg}$  and  $\omega_{fe}$  fluctuations changes from negative to positive.

With time-energy entangled photons produced by spontaneous parametric down-conversion (SPDC) pumped by a narrowband source, we find that the one-photon resonant peaks in the fast modulation limit are eliminated and the dependence of the spectra on the correlation between fluctuations is suppressed due to the

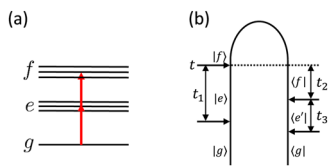


**FIG. 1.** (a) A three-band system with the ground  $g$ , intermediate  $e$ , and final  $f$  states. Only the transitions between  $g$  and  $e$  and between  $e$  and  $f$  are electric dipole allowed. (b) Loop diagram representing the TPA process in Hilbert space. Incoming arrows denote photon absorption. For diagrammatic rules, see Ref. 27.

broad one-photon but narrow two-photon spectrum of the twin photons. ETPA can thus better resolve the  $g$ - $f$  transitions by suppressing interfering peaks caused by resonant intermediate states in CTPA. We further study the ETPA-induced coherences in the  $f$  manifold and find that correlated level fluctuations lead to stronger coherences due to the suppression of dephasing.

## II. THE MODEL

We consider a three-band electronic system diagonally coupled to a harmonic bath and described by the Hamiltonian,<sup>23</sup>

$$\begin{aligned} \hat{H} &= \sum_e |e\rangle\langle e|(\omega_{eg} + \hat{Q}_e) + \sum_f |f\rangle\langle f|(\omega_{fg} + \hat{Q}_f) + \hat{H}_B, \\ \hat{H}_B &= \sum_j \left( \frac{\hat{p}_j^2}{2m_j} + \frac{m_j \omega_j^2}{2} \hat{q}_j^2 \right), \\ \hat{Q}_s &= \sum_j c_{sj} \hat{q}_j. \end{aligned} \quad (1)$$

The electronic states form three bands [Fig. 1(a)]: ground state  $|g\rangle$ , one-photon absorption allowed intermediate states  $|e\rangle$ , and TPA allowed final states  $|f\rangle$ ; the ground state energy is set to 0;  $\omega_{ss'}$  ( $s, s' = g, e, f$ ) is the transition energy from  $s'$  to  $s$  at the ground state equilibrium geometry (Franck-Condon point); and  $\hat{Q}_s$  is a collective bath coordinate that modulates the  $|s\rangle$  state energy.

Within the rotating wave approximation, the light-matter dipole interaction is given by

$$\hat{H}_I(t) = -\hat{V}^\dagger(t)\hat{E}(t) + \text{h.c.}, \quad (2)$$

where  $\hat{V}^\dagger = \sum_e \mu_{eg} |e\rangle\langle g| + \sum_{e,f} \mu_{fe} |f\rangle\langle e|$  is the raising part of the transition dipole operator,  $\hat{E}(t) = \int_0^\infty d\omega \sqrt{\frac{\hbar\omega}{4\pi\epsilon_0 c A}} \hat{a}(\omega) e^{-i\omega t}$  is the positive frequency component of the electric field operator,  $\hat{a}(\omega)$  is the photon annihilation operator that satisfies  $[\hat{a}(\omega), \hat{a}^\dagger(\omega')] = \delta(\omega - \omega')$ ,  $c$  is the light velocity, and  $A$  is the effective area of the light beam.

## III. THE TPA SIGNAL

The TPA signal is given by the  $f$ -state population induced by the pump pulse,

$$P_f \stackrel{t \rightarrow \infty}{=} \text{Tr} \left[ \hat{\rho}(t) \sum_f |f\rangle\langle f| \right], \quad (3)$$

where  $\hat{\rho}(t) = \mathcal{T} e^{-i \int_{-\infty}^t dt' \hat{H}_I(t')} \hat{\rho}(-\infty) \tilde{\mathcal{T}} e^{i \int_{-\infty}^t dt'' \hat{H}_I(t'')}$  and  $\hat{\rho}(-\infty) = |g\rangle\langle g| \otimes e^{-\frac{\hat{H}_B}{k_B T}} \otimes \hat{\rho}_E$ . Here,  $\mathcal{T}$  and  $\tilde{\mathcal{T}}$  are time ordering and

anti-time ordering super-operators, respectively, and we assume that initially the material system is in the ground state thermal equilibrium and the field density matrix is  $\hat{\rho}_E$ . Fourth order perturbative expansion of  $\hat{\rho}(t)$  in  $\hat{H}_I$  represented by the loop diagram shown in Fig. 1(b) gives

$$\begin{aligned} P_f &= \text{Tr} \left[ \int_{-\infty}^{+\infty} dt' \int_{-\infty}^{t'} dt'' \hat{H}_I(t') \hat{H}_I(t'') \hat{\rho}(-\infty) \right. \\ &\quad \left. \times \int_{-\infty}^{+\infty} dt''' \int_{-\infty}^{t'''} dt'''' \hat{H}_I(t''') \hat{H}_I(t''') \sum_f |f\rangle\langle f| \right] \\ &= 2\text{Re} \int_{-\infty}^{+\infty} dt \int_0^{+\infty} dt_{1 \sim 3} \langle \hat{V}(t_1 - t_2 - t_3) \hat{V}(t_1 - t_2) \hat{V}^\dagger(t_1) \\ &\quad \hat{V}^\dagger(0) \rangle \times \langle \hat{E}^\dagger(t - t_2 - t_3) \hat{E}^\dagger(t - t_2) \hat{E}(t) \hat{E}(t - t_1) \rangle. \quad (4) \end{aligned}$$

By imposing complete time ordering between light-matter interactions on the bra and ket sides, one can decompose this loop diagram into three ladder diagrams (see Appendix A).<sup>26</sup> Normally one would apply ladder diagrams to take bath effects into account, but here the loop diagram is sufficient since the diagonal Gaussian fluctuation model allows for the evaluation of matter correlation functions with a general time ordering [see Eqs. (5) and (6)]. The loop diagram yields a more compact expression and is easier to implement numerically.

### A. The matter correlation functions

The exact matter correlation functions for the model in Eq. (1) can be obtained by second-order cumulant expansion (known as cumulant expansion of Gaussian fluctuations),<sup>28</sup>

$$\begin{aligned} &\langle \hat{V}(t_4) \hat{V}(t_3) \hat{V}^\dagger(t_2) \hat{V}^\dagger(t_1) \rangle \\ &= \sum_{e'e'f} \mu_{e'g}^* \mu_{f'e'}^* \mu_{fe} \mu_{eg} \exp \left[ -i(\omega_{e'g} \tau_{43} + \omega_{fg} \tau_{32} + \omega_{eg} \tau_{21}) \right. \\ &\quad \left. + \phi_{e'feg}(t_4, t_3, t_2, t_1) \right] \end{aligned} \quad (5)$$

with  $\mu_{ss'} = \langle s | \hat{V}^\dagger | s' \rangle$ ,  $\tau_{ij} = t_i - t_j$ , and

$$\begin{aligned} \phi_{e'feg}(t_4, t_3, t_2, t_1) &= -g_{e'e'}(\tau_{43}) - g_{ff}(\tau_{32}) - g_{ee}(\tau_{21}) \\ &\quad - g_{e'f}(\tau_{42}) + g_{e'f}(\tau_{43}) + g_{e'f}(\tau_{32}) \\ &\quad - g_{e'e}(\tau_{41}) + g_{e'e}(\tau_{42}) + g_{e'e}(\tau_{31}) \\ &\quad - g_{e'e}(\tau_{32}) - g_{fe}(\tau_{31}) + g_{fe}(\tau_{32}) + g_{fe}(\tau_{21}). \end{aligned} \quad (6)$$

The line-shape function  $g_{vv'}$ ( $t$ ) is defined as

$$g_{vv'}(t) = \int_0^t dt_2 \int_0^{t_2} dt_1 C_{vv'}(t_2 - t_1), \quad (7)$$

where  $C_{vv'}(t_2 - t_1) = \langle \hat{Q}_v(t_2) \hat{Q}_{v'}(t_1) \rangle$  is the correlation function of the bath-induced level fluctuations whose time evolution is governed by the bath Hamiltonian,  $\hat{Q}_v(t) = e^{i\hat{H}_B t} \hat{Q}_v e^{-i\hat{H}_B t}$ . The line-shape function can also be expressed in terms of the spectral density  $C_{vv'}''(\omega)$ ,

$$g_{vv'}(t) = \int \frac{d\omega}{2\pi} \frac{C_{vv'}''(\omega)}{\omega^2} \left[ \coth\left(\frac{\beta\hbar\omega}{2}\right) (1 - \cos \omega t) + i \sin \omega t - i\omega t \right] \quad (8)$$

with  $\beta = 1/(k_B T)$  and

$$C''_{\nu\nu'}(\omega) = \frac{1}{2} \int_0^\infty dt e^{i\omega t} \langle [\hat{Q}_\nu(t), \hat{Q}_{\nu'}(0)] \rangle. \quad (9)$$

Hereafter, we adopt the over-damped Brownian oscillator spectral density

$$C''_{\nu\nu'}(\omega) = 2\lambda_{\nu\nu'} \frac{\omega\Lambda}{\omega^2 + \Lambda^2}, \quad (10)$$

where  $\Lambda^{-1}$  is the fluctuation timescale and  $\lambda_{\nu\nu'}$  characterizes system–bath coupling strength. The corresponding line-shape function for  $t > 0$  and high temperature  $T \gg \Lambda$  is

$$g_{\nu\nu'}(t) = \frac{\lambda_{\nu\nu'}}{\Lambda} \left( \frac{2}{\hbar\Lambda\beta} - i \right) [\exp(-\Lambda t) + \Lambda t - 1]. \quad (11)$$

For  $t < 0$ ,  $g_{\nu\nu'}(t) = g_{\nu\nu'}^*(-t)$ . We introduce a dimensionless parameter  $\kappa_{\nu\nu'} \equiv \left( \frac{\hbar\Lambda^2}{2\lambda_{\nu\nu'}k_B T} \right)^{1/2}$  to define the fast ( $\kappa \gg 1$ ) and slow ( $\kappa \ll 1$ ) bath modulation limits, whereby the fluctuation timescale  $\Lambda^{-1}$  is faster or slower than the fluctuation magnitude  $\sqrt{2\lambda_{\nu\nu'}k_B T/\hbar}$ . Hereafter, we set  $\kappa_{\nu\nu'} \equiv \kappa$  and  $\lambda_{\nu\nu'} \equiv \lambda$  for all states and fix the

linewidth (FWHM) while varying  $\kappa$  via the Padé approximation,<sup>29</sup>

$$\frac{\text{FWHM}}{\sqrt{2\lambda k_B T/\hbar}} = \frac{2.355 + 1.76\kappa}{1 + 0.85\kappa + 0.88\kappa^2}. \quad (12)$$

We thus vary  $\lambda$  and  $\Lambda$  simultaneously. Another dimensionless parameter  $\eta_{\nu\nu'} = \lambda_{\nu\nu'}/\sqrt{\lambda_{\nu\nu'}\lambda_{\nu'\nu'}}$  characterizes the correlation between energy fluctuations of levels  $\nu$  and  $\nu'$ ,<sup>30</sup> which are fully anti-correlated for  $\eta_{\nu\nu'} = -1$ , uncorrelated for  $\eta_{\nu\nu'} = 0$ , and fully correlated for  $\eta_{\nu\nu'} = 1$ .

## B. The field correlation functions

The field correlation function in Eq. (4) depends on the nature of the light. For classical fields, it simply factorizes,

$$\langle \hat{E}^\dagger(t_4)\hat{E}^\dagger(t_3)\hat{E}(t_2)\hat{E}(t_1) \rangle = E^*(t_4)E^*(t_3)E(t_2)E(t_1). \quad (13)$$

For entangled photons produced by degenerate type-II spontaneous parametric down-conversion (SPDC), the normalized twin-photon state is<sup>20,31</sup>

$$|\Psi\rangle = \left( \frac{T_p T_e}{\pi\sqrt{\pi/2}} \right)^{1/2} \int d\omega_1 d\omega_2 \exp\{-T_p^2(\omega_1 + \omega_2 - 2\omega_0)^2\} \times \text{sinc}\left(\frac{\omega_2 - \omega_1}{2} T_e\right) \hat{a}_1^\dagger(\omega_1)\hat{a}_2^\dagger(\omega_2)|0\rangle, \quad (14)$$

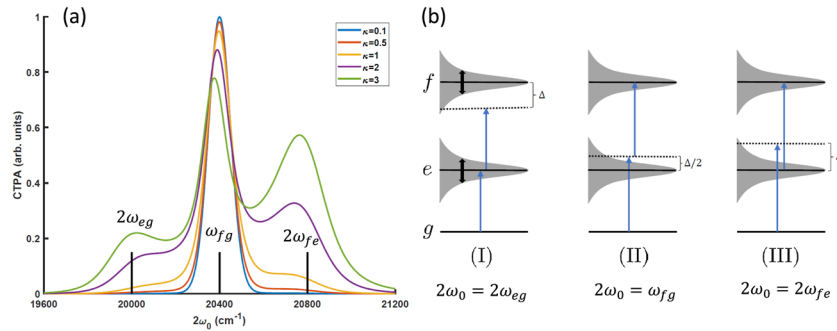


**FIG. 2.** (a) CTPA signals of a three-level system coupled to an over-damped Brownian oscillator bath. The bath timescale is changed by varying parameter  $\kappa$  while keeping FWHM fixed to  $100 \text{ cm}^{-1}$  [see Eq. (12)]. As the energy modulation changes from slow to fast ( $\kappa$  increases), one-photon resonant peaks appear because of the long tail of the Lorentzian line shape at fast modulation compared to the short tail of the Gaussian line shape at slow modulation; redshift of the central peak is due to the imaginary part of the  $g$  function. A classical narrowband pulse  $E(t) = E_p \exp(-\sigma_p^2/4t^2 - i\omega_0 t)$  is used. The parameters are  $\omega_{eg} = 10\,000 \text{ cm}^{-1}$ ,  $\omega_{fg} = 20\,400 \text{ cm}^{-1}$ ,  $\mu_{fg} = \mu_{eg}$ ,  $\eta_{ef} = 0.5$ ,  $T = 417 \text{ cm}^{-1}$ , and  $\sigma_p = 37.5 \text{ cm}^{-1}$ . (b) Various resonance scenarios that result in the three peaks in the CTPA signal: (I)  $g$ - $e$  is one-photon resonant; (II)  $g$ - $f$  is two-photon resonant; and (III)  $e$ - $f$  is one-photon resonant.  $\Delta = \omega_{fg} - \omega_{eg}$ . Gray shapes represent line broadening due to energy level fluctuations.

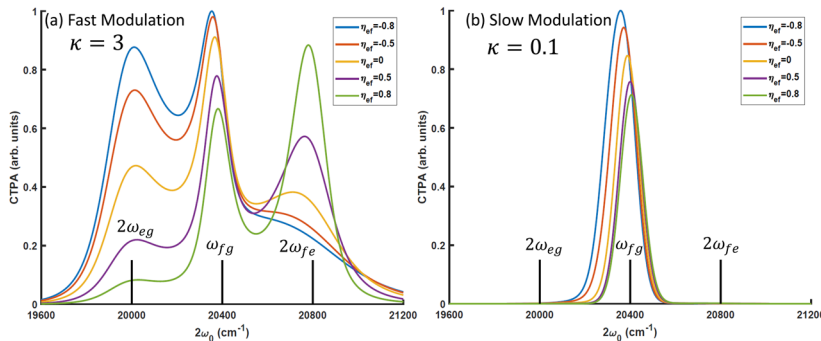


**FIG. 3.** CTPA signals vary with the correlation between level fluctuations of  $e$  and  $f$ . (a) In the fast modulation limit, the  $2\omega_{eg}$  peak is weakened, whereas the  $2\omega_{fe}$  peak is strengthened and sharpened as the correlation gradually becomes positive. Meanwhile, the  $g$ - $f$  peak is slightly blueshifted. (b) In the slow modulation limit, the  $g$ - $f$  peak position and intensity change with the correlation.

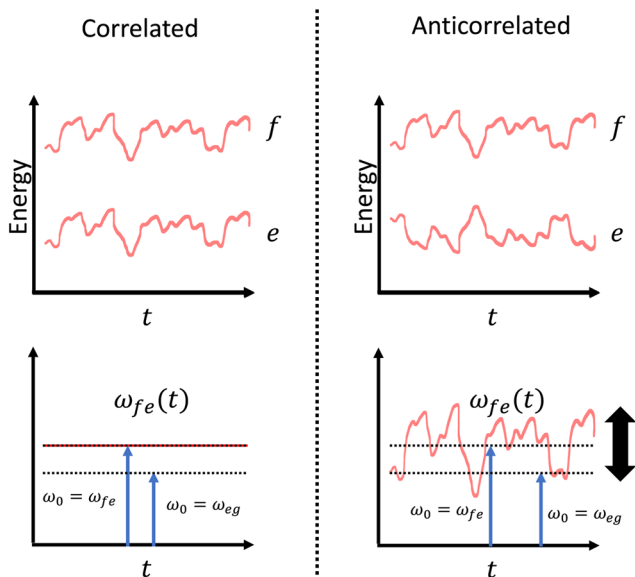


**FIG. 4.** Mechanism of correlation-induced narrowing and enhancement of the  $2\omega_{fe}$  peak and weakening of the  $2\omega_{eg}$  peak in CTPA signals. The bath introduces time-dependent fluctuations of the energy levels. When the energy fluctuations of level  $e$  and  $f$  are correlated, the fluctuations cancel each other in the transition energy  $\omega_{fe}(t)$ , and thus  $\omega_{fe}(t)$  is narrowly distributed around its mean value  $\omega_{fe}$  and away from  $\omega_{eg}$ . As a result, photons of frequency  $\omega_{fe}$  are strongly absorbed and the  $2\omega_{fe}$  peaks are narrow, whereas those of frequency  $\omega_{eg}$  are weakly absorbed. In contrast, when the energy fluctuations are anti-correlated, they add up in the transition energy  $\omega_{fe}$ , and thus,  $\omega_{fe}$  is widely distributed and detuned from its mean value most of the time. As a result, the absorption of photons of frequency  $\omega_{fe}$  is weakened and the  $2\omega_{fe}$  peaks are broad; meanwhile, the absorption of those of frequency  $\omega_{eg}$  is enhanced.

where  $T_p$  is the SPDC pump duration,  $2\omega_0$  is the pump central frequency, and  $T_e$  is the entanglement time. The exponential term describes the frequency anticorrelation of the twin photons:  $\omega_1 + \omega_2 \approx 2\omega_0$ . The field correlation function for

ETPA is

$$\langle \hat{E}^\dagger(t_4)\hat{E}^\dagger(t_3)\hat{E}(t_2)\hat{E}(t_1) \rangle = \langle \Psi | \hat{E}^\dagger(t_4)\hat{E}^\dagger(t_3) | 0 \rangle \times \langle 0 | \hat{E}(t_2)\hat{E}(t_1) | \Psi \rangle \quad (15)$$

with

$$\langle 0 | \hat{E}(t_2)\hat{E}(t_1) | \Psi \rangle = \frac{\hbar\omega_0}{2(2\pi)^{1/4}\epsilon_0 c A \sqrt{T_e T_p}} \Pi\left(\frac{t_2 - t_1}{2T_e}\right) \times e^{-(t_1+t_2)^2/16T_p^2 - i\omega_0 t_1 - i\omega_0 t_2}, \quad (16)$$

where  $\Pi(\cdot)$  is the rectangular function:  $\Pi(x) = 1/2$  for  $-1/2 < x < 1/2$  and 0 otherwise, and it ensures that two photons arrive together within  $T_e$ .

### C. TPA of a three-level model

We consider CTPA [Fig. 2(a)] of a three-level system with a nearly resonant intermediate state:  $\omega_{eg} \approx \omega_{fe}$  in Fig. 1(a). As the level modulation by the bath becomes fast ( $\kappa$  increases), side peaks appear at  $2\omega_{eg}$  and  $2\omega_{fe}$ , and the  $\omega_{fg}$  peak is redshifted. The redshift (known as the reorganization energy) is due to the imaginary part of the line-shape function in the fast modulation limit:  $\text{Im } g_{vv}(t) = -\lambda t$ . The three peaks in this case correspond to the three resonant scenarios shown in Fig. 2(b). In case (I), the incoming light is one-photon resonant with  $\omega_{eg}$  but off-resonant with  $\omega_{fe}$  by  $\Delta = \omega_{fe} - \omega_{eg}$ ; in case (II), the incoming light is two-photon resonant with  $\omega_{fg}$  but one-photon off-resonant with  $\omega_{eg}$  and  $\omega_{fe}$  by  $\Delta/2$ ; and in case (III), the incoming light is one-photon resonant with  $\omega_{fe}$  but off-resonant with  $\omega_{eg}$  by  $\Delta$ . Because of the long tail of the Lorentzian line shape for fast level modulations, the contribution of cases (I) and (III) to the signal are comparable to that of case (II). In the slow modulation limit, in contrast, cases (I) and (III) are much weaker than case (II) because of the sharp tail of the Gaussian

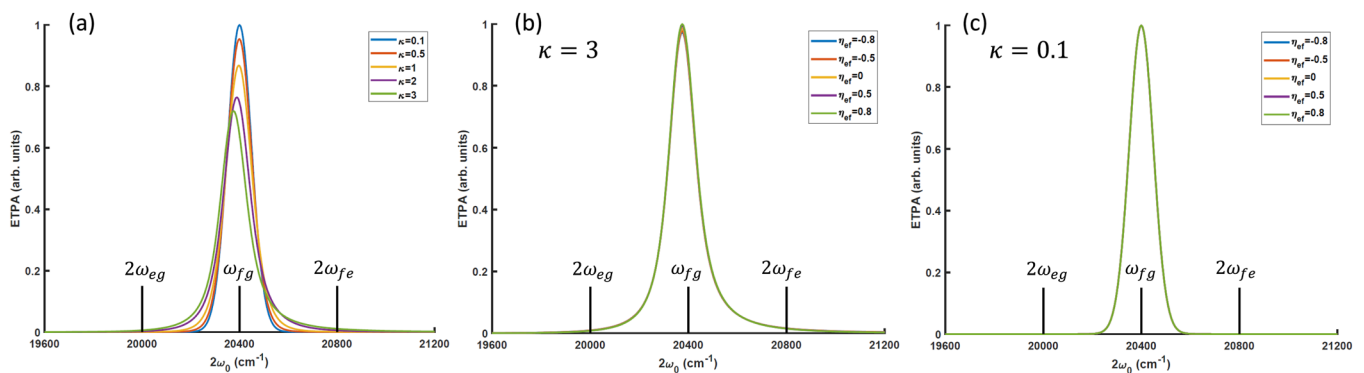


**FIG. 5.** ETPA signals of a three-level system [Fig. 2(b)]. (a) Transition from slow ( $\kappa = 0.1$ ) to fast ( $\kappa = 3$ ) bath modulations. The change of the line shape from Gaussian to Lorentzian and the redshift of the peak are clearly demonstrated.  $\eta_{ef} = 0.5$ . (b) and (c) correspond to ETPA signals in the fast and slow modulation limits with varying correlations between energy fluctuations of  $e$  and  $f$ . Compared to CTPA spectra in Figs. 2 and 3, one-photon resonant peaks disappear and the spectra are independent of the correlation between energy fluctuations of  $e$  and  $f$ . Both effects are due to the peculiar spectrum of the entangled photon pairs: one-photon broadband but two-photon narrowband.  $T_p = 100$  fs and  $T_e = 10$  fs. Other parameters are the same as in Fig. 2.

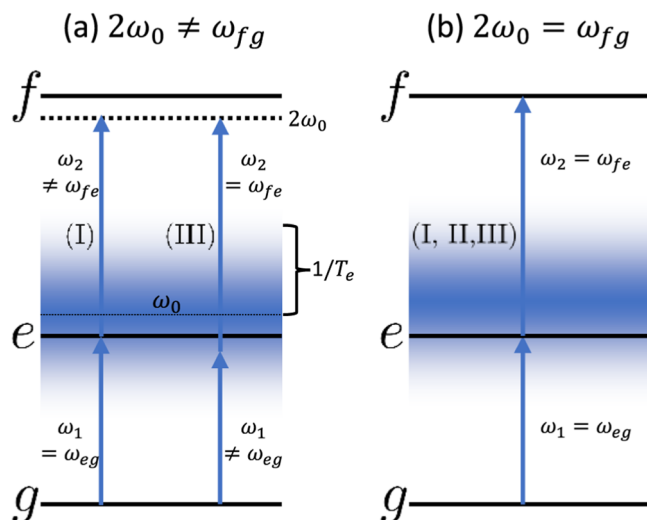


**FIG. 6.** Elimination of the extra one-photon resonant peaks in the ETPA signal due to the peculiar spectrum of the entangled photons. Blue shades represent the spectrum of single photons in the pair. For a short entanglement time  $T_e$ , both  $g$ - $e$  and  $e$ - $f$  transitions are within the single photon energy bandwidth ( $\sim \hbar/T_e$ ). Therefore, the resonant conditions for cases (I) and (III) in Fig. 2(b) are always met regardless of the pump frequency. (a) When the SPDC pump frequency is off-resonant with the  $g$ - $f$  transition ( $2\omega_0 \neq \omega_{fg}$ ),  $g$ - $e$  and  $e$ - $f$  transitions cannot both be excited resonantly due to the frequency anticorrelation  $\omega_1 + \omega_2 = 2\omega_0$ . (b) When the SPDC pump frequency is resonant with the  $g$ - $f$  transition ( $2\omega_0 = \omega_{fg}$ ), the two photons can be resonant with  $g$ - $e$  and  $e$ - $f$  transitions, respectively, i.e., the resonant conditions for cases (I), (II), and (III) are simultaneously achieved. Such double resonances cannot be achieved in (a), and therefore, the signal is greatly enhanced.

line shape and the smaller energy mismatch in case (II). The extra one-photon resonant peaks thus only appear in the fast modulation limit.

We next turn to the CTPA variation with the degrees of correlation between fluctuations. Figure 3(a) shows that for

fast modulation, the  $2\omega_{eg}$  peak is weakened, but the  $2\omega_{fe}$  peak is strengthened and sharpens as the parameter  $\eta_{ef}$  is varied such that the energy fluctuations of  $e$  and  $f$  change from being anti-correlated ( $\eta_{ef} < 0$ ) to correlated ( $\eta_{ef} > 0$ ). This is because when the fluctuations of levels  $e$  and  $f$  are correlated, the  $e$ - $f$  transition energy remains close to its mean value  $\omega_{fe}$  (see Fig. 4). The narrow distribution strengthens the absorption of a photon with frequency  $\omega_{fe}$  but weakens the absorption of a  $\omega_{eg}$  photon. In contrast, for anti-correlated fluctuations, their magnitudes add up in the fluctuations of the energy difference, and the  $e$ - $f$  transition energy has a broad distribution, which, in turn, causes a weaker and broader  $2\omega_{fe}$  peak but a stronger  $2\omega_{eg}$  peak. See also Appendix B for a mathematical explanation. Note that for both fast [Fig. 3(a)] and slow [Fig. 3(b)] modulations, the  $g$ - $f$  peak is blueshifted as the fluctuations become more positively correlated. This is because the  $e$ - $f$  transition is higher in energy than  $g$ - $e$  and is increasingly dominating.

The extra one-photon resonant CTPA peaks complicate the signal interpretation as they are close to the  $g$ - $f$  transitions. In ETPA with a short entanglement time (Fig. 5), however, the one-photon resonant peaks vanish and the dependence of the  $g$ - $f$  peak on correlation between level fluctuations is diminished because of the specific spectrum of the entangled photons (see Fig. 6). Although the two-photon frequency is narrowly distributed with bandwidth  $\sim \hbar/T_p$ , each photon is individually broad with bandwidth  $\sim \hbar/T_e$ .<sup>17</sup> Therefore, for a short entanglement time  $T_e$ ,  $g$ - $e$  and  $e$ - $f$  transitions both lie within the single photon spectrum (approximately from  $\omega_0 - \hbar/T_e$  to  $\omega_0 + \hbar/T_e$ ) regardless of the SPDC pump frequency, i.e., the resonant conditions for cases (II) and (III) in Fig. 2 are always satisfied. ETPA is sensitive to the final state energy but not to energies of the intermediate resonant states.

#### D. TPA of a multi-level system

In the CTPA spectra of the five-level system shown in Fig. 7, we see the one-photon resonant peaks as the energy modulations

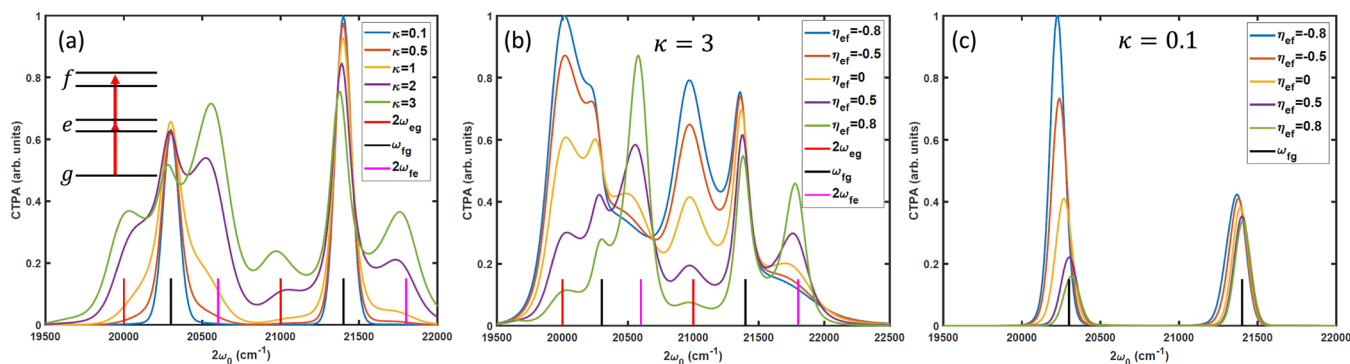


**FIG. 7.** CTPA spectra of a five-level system with one  $g$ , two  $e$ , and two  $f$  states. (a) One-photon resonant peaks appear as the energy modulation becomes fast. Two-photon frequencies that satisfy different resonant conditions shown in Fig. 2(b) are denoted as vertical bars with different colors.  $\eta_{ef} = 0.5$ . (b) For fast modulation ( $\kappa = 3$ ),  $2\omega_{eg}$  peaks are weakened, but  $2\omega_{fe}$  peaks are enhanced and sharpened as the correlations between energy fluctuations of states  $e$  and  $f$  become more positively correlated. (c) For slow modulation ( $\kappa = 0.1$ ), the positions and intensities of  $g$ - $f$  peaks change with the correlations. The parameters are  $\omega_{eg} \in \{10\,000, 10\,500\} \text{ cm}^{-1}$ ,  $\omega_{fg} \in \{20\,300, 21\,400\} \text{ cm}^{-1}$ ,  $\eta_{eef} = 0.9$ ,  $\sigma_p = 37.5 \text{ cm}^{-1}$ , and  $T = 417 \text{ cm}^{-1}$ .

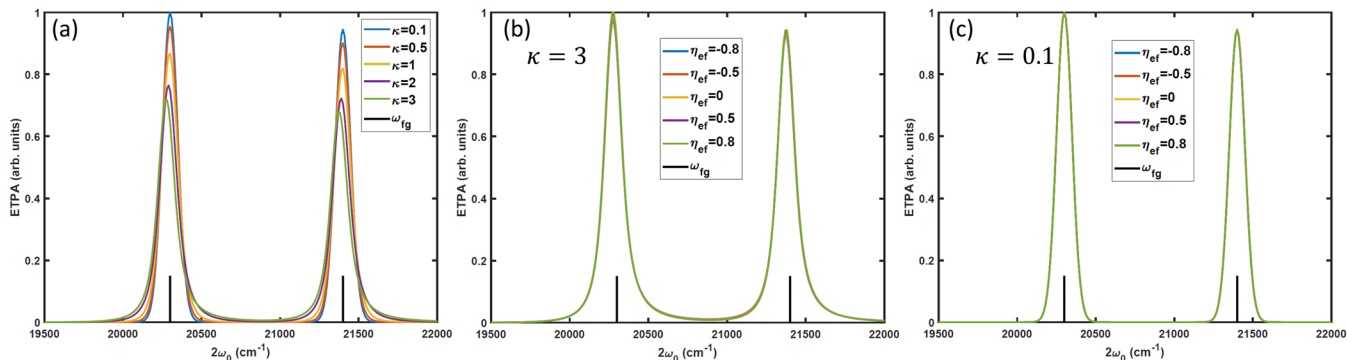


**FIG. 8.** ETPA spectra of the five-level system in Fig. 7. (a) Transition from slow ( $\kappa = 0.1$ ) to fast ( $\kappa = 3$ ) bath modulations with fixed  $\eta_{ef} = 0.5$ . (b) and (c) correspond to fast and slow modulations with varying correlation between energy fluctuations of  $e$  and  $f$ . Compared to CTPA spectra in Fig. 7, one-photon resonant peaks disappear and the spectra dependence on correlation between fluctuations is suppressed. ETPA spectra show clear features of  $g$ - $f$  transitions.  $T_p = 100$  fs,  $T_e = 10$  fs. Other parameters are the same as in Fig. 7.

become fast, as well as the spectra variation with the correlations between energy fluctuations of the intermediate and final states. In particular, one-photon resonant peaks may sometimes be strong enough to obscure the  $g$ - $f$  peaks [see the blue line in Fig. 7(b)]. In contrast, only  $g$ - $f$  peaks are observed in the ETPA spectra shown in Fig. 8, and the redshift and line shape change from Gaussian to Lorentzian are clearly seen. The spectra dependence on the correlations between fluctuations is suppressed.

#### IV. ETPA-INDUCED COHERENCES BETWEEN $f$ STATES

So far, we have focused on  $f$  state populations created by TPA. Now, we investigate the ETPA-induced coherences between  $f$  states,<sup>32</sup> which under fourth order perturbative expansion in  $\hat{H}_I$  in

the interaction picture is given by

$$\begin{aligned} \hat{\rho}_{f'f'}(t) &= \text{Tr}[|f'\rangle\langle f|\hat{\rho}(t)] \\ &= \int_{-\infty}^t dt_2 \int_{-\infty}^{t_2} dt_1 \int_{-\infty}^t dt_3 \int_{-\infty}^{t_3} dt_4 \langle \hat{V}(t_4) \hat{V}(t_3) \\ &\quad \times |f'\rangle\langle f|(t) \hat{V}^\dagger(t_2) \hat{V}^\dagger(t_1) \\ &\quad \times \langle \hat{E}^\dagger(t_4) \hat{E}^\dagger(t_3) \hat{E}(t_2) \hat{E}(t_1) \rangle. \end{aligned} \quad (17)$$

Using the second-order cumulant expansion, which is exact for our model, the matter correlation function is given by

$$\begin{aligned} &\langle \hat{V}(t_5) \hat{V}(t_4) |f'\rangle\langle f|(t_3) \hat{V}^\dagger(t_2) \hat{V}^\dagger(t_1) \rangle \\ &= \sum_{ee'} \mu_{e'g}^* \mu_{f'e'}^* \mu_{fe} \mu_{eg} \exp[-i(\omega_{e'g} \tau_{54} + \omega_{f'g} \tau_{43} \\ &\quad + \omega_{fg} \tau_{32} + \omega_{eg} \tau_{21}) + \phi_{e'f'feg}(t_5, t_4, t_3, t_2, t_1)] \end{aligned} \quad (18)$$

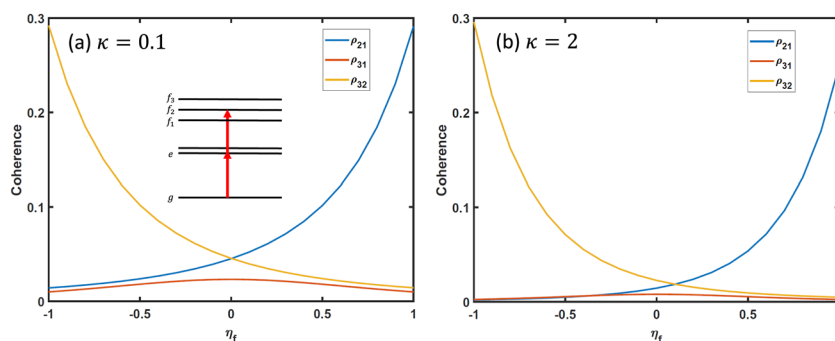


**FIG. 9.** ETPA-induced  $f$ -state coherences vary with the correlations between  $f$ -state energy fluctuations for a six-level system with one  $g$ , two  $e$ , and three  $f$  states. (a) and (b) correspond to slow and fast bath modulations. The y-axis value is the magnitude of the coherence normalized with respect to total  $f$ -state population. The coherence is evaluated at  $t = 4T_p$ . The parameters are  $\omega_{eg} \in \{10\,000, 10\,500\}$   $\text{cm}^{-1}$ ,  $\omega_{f_1g} = 20\,300$   $\text{cm}^{-1}$ ,  $\omega_{f_2g} = 20\,400$   $\text{cm}^{-1}$ ,  $\omega_{f_3g} = 20\,500$   $\text{cm}^{-1}$ ,  $T = 417$   $\text{cm}^{-1}$ ,  $T_p = 50$  fs,  $T_e = 10$  fs,  $\eta_{ee'} = 0.9$ ,  $\eta_{ef} = 0$ ,  $\eta_{f_1f_2} = \eta_f$ ,  $\eta_{f_2f_3} = -\eta_f$ , and  $\eta_{f_1f_3} = -\eta_f^2$ .  $\rho_{ab}$  in the figure denotes the coherence between  $a$ th and  $b$ th  $f$  states. As  $\eta_f$  increases, energy fluctuations of  $f_1$  and  $f_2$  become more correlated, and therefore, their coherence  $\rho_{21}$  is strengthened due to suppression of dephasing. On the other hand, the coherence  $\rho_{32}$  between  $f_2$  and  $f_3$  is weakened due to increasingly more anti-correlated fluctuations. The coherence  $\rho_{13}$  between  $f_1$  and  $f_3$  stays small because their energy fluctuations remain anti-correlated.

$$\begin{aligned} \phi_{e'f'feg}(t_5, t_4, t_3, t_2, t_1) = & -g_{e'e'}(\tau_{54}) - g_{f'f'}(\tau_{43}) - g_{ff}(\tau_{32}) \\ & - g_{ee}(\tau_{21}) - g_{e'f'}(\tau_{53}) + g_{e'f'}(\tau_{54}) + g_{e'f'}(\tau_{43}) \\ & - g_{f'f}(\tau_{42}) + g_{f'f}(\tau_{43}) + g_{f'f}(\tau_{32}) - g_{fe}(\tau_{31}) \\ & + g_{fe}(\tau_{21}) + g_{fe}(\tau_{32}) - g_{e'f}(\tau_{52}) + g_{e'f}(\tau_{53}) \\ & + g_{e'f}(\tau_{42}) - g_{e'f}(\tau_{43}) - g_{f'e}(\tau_{41}) + g_{f'e}(\tau_{42}) \\ & + g_{f'e}(\tau_{31}) - g_{f'e}(\tau_{32}) - g_{e'e}(\tau_{51}) + g_{e'e}(\tau_{52}) + g_{e'e}(\tau_{41}) - g_{e'e}(\tau_{42}). \end{aligned} \quad (19)$$

Figure 9 depicts the variation of various  $f$ -state coherences with the correlation between  $f$ -state energy fluctuations for a six-level system. We find that correlated fluctuations strengthen the coherences in the  $f$  manifold because it suppresses the fluctuation of frequency difference between  $f$  states and thus reduce the dephasing rate. In Appendix C, we show that the  $f$ -state coherences do not depend on correlation between fluctuations of  $\omega_{eg}$  and  $\omega_{fg}$  because ETPA is insensitive to the  $e$ -state energies.

## V. CONCLUSIONS

We have compared classical and entangled two-photon absorption for the Brownian oscillator bath model, which is applicable to spectroscopy of solvated molecules. In the presence of (nearly) resonant intermediate states and for fast energy modulations, extra peaks appear around  $\omega_{fg}$  in CTPA, which correspond to one-photon resonant  $g$ - $e$  or  $e$ - $f$  transitions. The spectra strongly depend on the correlation between energy fluctuations of the  $e$  and  $f$  states.

One-photon resonant peaks make it difficult to resolve the  $g$ - $f$  transitions in the CTPA spectra. In ETPA, in contrast, the one-photon resonant peaks disappear and eventually only  $\omega_{fg}$  peaks are observed. The dependence of the spectra on the correlations between fluctuations is also suppressed. Both effects are due to the specific spectrum of the twin photons: broadband one-photon combined with narrowband two-photon frequency distributions. We expect to observe similar effects by replacing entangled photons with classical energy-correlated fields<sup>33</sup> since the latter also possess broad one-photon but narrow two-photon spectra. The ETPA-induced  $f$ -state coherences reflect the suppression of dephasing by correlated energy fluctuations.

## ACKNOWLEDGMENTS

The support of the NSF under Grant No. CHE-1953045 is gratefully acknowledged. S.M. was supported by the U.S. Department of Energy, Office of Science, Office of Basic Energy Sciences,

under Award No. DE-SC0022134 (S.M.). We thank Dr. Bing Gu for helpful discussions.

## AUTHOR DECLARATIONS

### Conflict of Interest

The authors have no conflicts of interest to disclose.

## DATA AVAILABILITY

The data that support the findings of this study are available from the corresponding author upon reasonable request.

## APPENDIX A: DECOMPOSITION OF THE LOOP DIAGRAM INTO LADDER DIAGRAMS

By imposing the complete time ordering between interactions on both sides of the loop diagram, i.e., by sorting  $\tau_1, \tau_2$ , and  $\tau_2 + \tau_3$  in Fig. 10, the loop diagram for the wavefunction in Hilbert space is decomposed into three ladder diagrams representing the density matrix in Liouville space,

$$\begin{aligned} S &= S_1 + S_2 + S_3, \\ S &= \int_{-\infty}^{+\infty} dt \int_0^{+\infty} d\tau_{1\sim 3} \langle \hat{V}(t - \tau_2 - \tau_3) \hat{V}(t - \tau_2) \hat{V}^\dagger(t) \hat{V}^\dagger(t - \tau_1) \rangle \\ &\quad \times \langle \hat{E}^\dagger(t - \tau_2 - \tau_3) \hat{E}^\dagger(t - \tau_2) \hat{E}(t) \hat{E}(t - \tau_1) \rangle, \\ S_1 &= \int_{-\infty}^{+\infty} dt \int_0^{+\infty} d\tau_{1\sim 3} \langle \hat{V}(t_1 + t_2) \hat{V}(t_1 + t_2 + t_3) \hat{V}^\dagger(t_1) \hat{V}^\dagger(0) \rangle \\ &\quad \times \langle \hat{E}^\dagger(t - t_3) \hat{E}^\dagger(t) \hat{E}(t - t_3 - t_2) \hat{E}(t - t_3 - t_2 - t_1) \rangle, \\ S_2 &= \int_{-\infty}^{+\infty} dt \int_0^{+\infty} d\tau_{1\sim 3} \langle \hat{V}(t_1) \hat{V}(t_1 + t_2 + t_3) \hat{V}^\dagger(t_1 + t_2) \hat{V}^\dagger(0) \rangle \\ &\quad \times \langle \hat{E}^\dagger(t - t_3 - t_2) \hat{E}^\dagger(t) \hat{E}(t - t_3) \hat{E}(t - t_3 - t_2 - t_1) \rangle, \\ S_3 &= \int_{-\infty}^{+\infty} dt \int_0^{+\infty} d\tau_{1\sim 3} \langle \hat{V}(t_1) \hat{V}(t_1 + t_2) \hat{V}^\dagger(t_1 + t_2 + t_3) \hat{V}^\dagger(0) \rangle \\ &\quad \times \langle \hat{E}^\dagger(t - t_3 - t_2) \hat{E}^\dagger(t - t_3) \hat{E}(t) \hat{E}(t - t_3 - t_2 - t_1) \rangle. \end{aligned} \quad (A1)$$

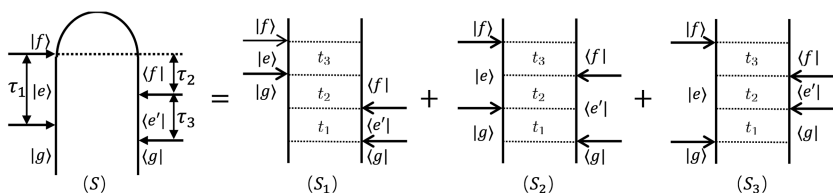
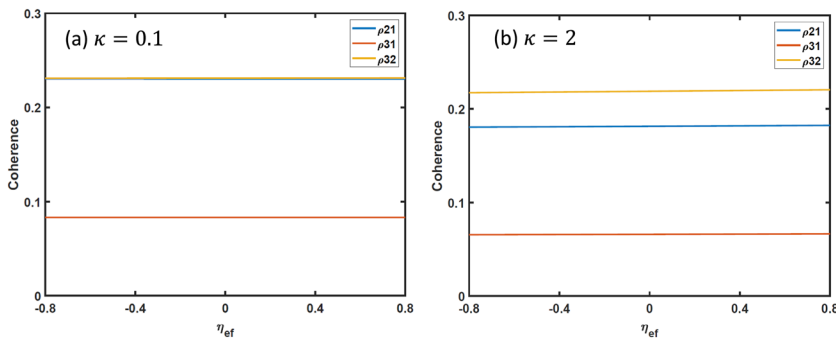


FIG. 10. Decomposition of the loop diagram ( $S$ ) for the two-photon absorption into three ladder diagrams ( $S_1$ - $S_3$ ) in Eq. (A1).



**FIG. 11.** *f*-state coherences vary with correlations between fluctuations of  $\omega_{eg}$  and  $\omega_{fg}$  for the six-level system in Figs. 9(a) and 9(b) correspond to slow and fast bath modulations.  $\eta_{ee'} = \eta_{ff'} = 0.9$ . Other parameters are the same as in Fig. 9.

## APPENDIX B: EXPLANATION OF THE ENHANCEMENT AND NARROWING OF $2\omega_{fe}$ PEAKS IN CTPA SIGNALS

In the fast modulation limit  $\kappa \gg 1$ ,

$$g_{vv'}(t) = \Gamma_{vv'} t - i\lambda_{vv'} t \quad (\text{B1})$$

with  $\Gamma_{vv'} \equiv \frac{\lambda_{vv'} k_B T}{\hbar \Lambda}$ . Plugging the above equation into Eq. (6) and using Eqs. (5) and (A1), we have for a classical continuous-wave pulse  $E(t) = E_p e^{-i\omega_0 t}$

$$\begin{aligned} S_1 &= |E_p|^4 \sum_{ee'ff'} \frac{\mu_{e'g}^* \mu_{fe'}^* \mu_{fe} \mu_{eg}}{[\Gamma_{ee} + i(E_{eg}^0 - \omega_0)][\Gamma_{ff} + i(E_{fg}^0 - 2\omega_0)]} \\ &\quad \times \frac{1}{(\Gamma_{e'e'} + \Gamma_{ff} - 2\Gamma_{e'f}) + i(E_{f'e'}^0 - \omega_0)}, \\ S_2 &= |E_p|^4 \sum_{ee'ff'} \frac{\mu_{e'g}^* \mu_{fe'}^* \mu_{fe} \mu_{eg}}{[\Gamma_{ee} + i(E_{eg}^0 - \omega_0)][\Gamma_{ee} + \Gamma_{e'e'} - 2\Gamma_{ee'} + iE_{ee'}^0]} \\ &\quad \times \frac{1}{(\Gamma_{e'e'} + \Gamma_{ff} - 2\Gamma_{e'f}) + i(E_{f'e'}^0 - \omega_0)}, \\ S_3 &= |E_p|^4 \sum_{ee'ff'} \frac{\mu_{e'g}^* \mu_{fe'}^* \mu_{fe} \mu_{eg}}{[\Gamma_{ee} + i(E_{eg}^0 - \omega_0)][\Gamma_{ee} + \Gamma_{e'e'} - 2\Gamma_{ee'} + iE_{ee'}^0]} \\ &\quad \times \frac{1}{(\Gamma_{ee} + \Gamma_{ff} - 2\Gamma_{ef}) + i(\omega_0 - E_{fe}^0)}. \end{aligned} \quad (\text{B2})$$

The last Lorentzian terms in the above expressions have width  $\Gamma_{ee} + \Gamma_{ff} - 2\eta_{ef} \sqrt{\Gamma_{ee}\Gamma_{ff}}$  and height  $\frac{1}{\Gamma_{ee} + \Gamma_{ff} - 2\eta_{ef} \sqrt{\Gamma_{ee}\Gamma_{ff}}}$ , so as we vary  $\eta_{ef}$  from  $-1$  to  $1$ , the  $2\omega_{fe}$  peaks in CTPA spectra become narrower and stronger.

## APPENDIX C: DEPENDENCE OF ETPA-INDUCED *f*-STATE COHERENCES ON $\eta_{ef}$

Figure 11 shows that the ETPA-induced coherences between *f* states do not depend on the correlation between fluctuations of  $\omega_{eg}$  and  $\omega_{fg}$ . This is due to the insensitivity of ETPA to the intermediate state energies.

## REFERENCES

- M. Rumi and J. W. Perry, "Two-photon absorption: An overview of measurements and principles," *Adv. Opt. Photonics* **2**, 451–518 (2010).
- K. E. Dorfman, F. Schlawin, and S. Mukamel, "Nonlinear optical signals and spectroscopy with quantum light," *Rev. Mod. Phys.* **88**, 045008 (2016).

- S. Mukamel, M. Freyberger, W. Schleich, M. Bellini, A. Zavatta, G. Leuchs, C. Silberhorn, R. W. Boyd, L. L. Sánchez-Soto, A. Stefanov, M. Barbieri, A. Paterova, L. Krivitsky, S. Schwartz, K. Tamasaku, K. Dorfman, F. Schlawin, V. Sandoghdar, M. Raymer, A. Marcus, O. Varnavski, T. Goodson, Z.-Y. Zhou, B.-S. Shi, S. Asban, M. Scully, G. Agarwal, T. Peng, A. V. Sokolov, Z.-D. Zhang, M. S. Zubairy, I. A. Vartanyants, E. del Valle, and F. Laussy, "Roadmap on quantum light spectroscopy," *J. Phys. B: At., Mol. Opt. Phys.* **53**, 072002 (2020).
- S. Szoke, H. Liu, B. P. Hickam, M. He, and S. K. Cushing, "Entangled light–matter interactions and spectroscopy," *J. Mater. Chem. C* **8**, 10732–10741 (2020).
- J. Javanainen and P. L. Gould, "Linear intensity dependence of a two-photon transition rate," *Phys. Rev. A* **41**, 5088–5091 (1990).
- D.-I. Lee and T. Goodson, "Entangled photon absorption in an organic porphyrin dendrimer," *J. Phys. Chem. B* **110**, 25582–25585 (2006).
- N. P. Georgiades, E. S. Polzik, K. Edamatsu, H. J. Kimble, and A. S. Parkins, "Nonclassical excitation for atoms in a squeezed vacuum," *Phys. Rev. Lett.* **75**, 3426–3429 (1995).
- B. Gu and S. Mukamel, "Manipulating two-photon-absorption of cavity polaritons by entangled light," *J. Phys. Chem. Lett.* **11**, 8177–8182 (2020).
- A. Muthukrishnan, G. S. Agarwal, and M. O. Scully, "Inducing disallowed two-atom transitions with temporally entangled photons," *Phys. Rev. Lett.* **93**, 093002 (2004).
- F. Schlawin, K. E. Dorfman, B. P. Fingerhut, and S. Mukamel, "Suppression of population transport and control of exciton distributions by entangled photons," *Nat. Commun.* **4**, 1782 (2013).
- F. Chen and S. Mukamel, "Vibrational hyper-Raman molecular spectroscopy with entangled photons," *ACS Photonics* **8**, 2722–2727 (2021).
- J. P. Villabona-Monsalve, O. Varnavski, B. A. Palfey, and T. Goodson, "Two-photon excitation of flavins and flavoproteins with classical and quantum light," *J. Am. Chem. Soc.* **140**, 14562–14566 (2018).
- D. Tabakaev, M. Montagnese, G. Haack, L. Bonacina, J.-P. Wolf, H. Zbinden, and R. T. Thew, "Energy-time-entangled two-photon molecular absorption," *Phys. Rev. A* **103**, 033701 (2021).
- O. Varnavski, B. Pinsky, and T. Goodson, "Entangled photon excited fluorescence in organic materials: An ultrafast coincidence detector," *J. Phys. Chem. Lett.* **8**, 388–393 (2017).
- T. Landes, M. Allgaier, S. Merkouche, B. J. Smith, A. H. Marcus, and M. G. Raymer, "Experimental feasibility of molecular two-photon absorption with isolated time-frequency-entangled photon pairs," *Phys. Rev. Res.* **3**, 033154 (2021).
- K. M. Parzuchowski, A. Mikhaylov, M. D. Mazurek, R. N. Wilson, D. J. Lum, T. Gerrits, C. H. Camp, M. J. Stevens, and R. Jimenez, "Setting bounds on entangled two-photon absorption cross sections in common fluorophores," *Phys. Rev. Appl.* **15**, 044012 (2021).
- M. G. Raymer, T. Landes, and A. H. Marcus, "Entangled two-photon absorption by atoms and molecules: A quantum optics tutorial," *J. Chem. Phys.* **155**, 081501 (2021).
- M. G. Raymer, T. Landes, M. Allgaier, S. Merkouche, B. J. Smith, and A. H. Marcus, "How large is the quantum enhancement of two-photon absorption by time-frequency entanglement of photon pairs?," *Optica* **8**, 757–758 (2021).

- <sup>19</sup>A. Mikhaylov, R. N. Wilson, K. M. Parzuchowski, M. D. Mazurek, C. H. Camp, Jr., M. J. Stevens, and R. Jimenez, "Hot-band absorption can mimic entangled two-photon absorption," *J. Phys. Chem. Lett.* **2022**, 1489–1493.
- <sup>20</sup>R. d. J. León-Montiel, J. Svozilik, L. J. Salazar-Serrano, and J. P. Torres, "Role of the spectral shape of quantum correlations in two-photon virtual-state spectroscopy," *New J. Phys.* **15**, 053023 (2013).
- <sup>21</sup>A. Perdomo-Ortiz, J. R. Widom, G. A. Lott, A. Aspuru-Guzik, and A. H. Marcus, "Conformation and electronic population transfer in membrane-supported self-assembled porphyrin dimers by 2D fluorescence spectroscopy," *J. Phys. Chem. B* **116**, 10757–10770 (2012).
- <sup>22</sup>M. G. Vivas, L. De Boni, T. M. Cooper, and C. R. Mendonca, "Interpreting strong two-photon absorption of PE3 platinum acetylide complex: Double resonance and excited state absorption," *ACS Photonics* **1**, 106–113 (2014).
- <sup>23</sup>S. Mukamel, in *Principles of Nonlinear Optical Spectroscopy* (Oxford University Press, 1995), Chap. 6.
- <sup>24</sup>J. M. Hales, D. J. Hagan, E. W. Van Stryland, K. J. Schafer, A. R. Morales, K. D. Belfield, P. Pacher, O. Kwon, E. Zojer, and J. L. Bredas, "Resonant enhancement of two-photon absorption in substituted fluorene molecules," *J. Chem. Phys.* **121**, 3152–3160 (2004).
- <sup>25</sup>M. Drobizhev, N. S. Makarov, T. Hughes, and A. Rebane, "Resonance enhancement of two-photon absorption in fluorescent proteins," *J. Phys. Chem. B* **111**, 14051–14054 (2007).
- <sup>26</sup>S. Mukamel, "Partially-time-ordered Schwinger-Keldysh loop expansion of coherent nonlinear optical susceptibilities," *Phys. Rev. A* **77**, 023801 (2008).
- <sup>27</sup>C. A. Marx, U. Harbola, and S. Mukamel, "Nonlinear optical spectroscopy of single, few, and many molecules: Nonequilibrium Green's function QED approach," *Phys. Rev. A* **77**, 022110 (2008).
- <sup>28</sup>D. Abramavicius, B. Palmieri, D. V. Voronine, F. Šanda, and S. Mukamel, "Coherent multidimensional optical spectroscopy of excitons in molecular aggregates; quasiparticle versus supermolecule perspectives," *Chem. Rev.* **109**, 2350–2408 (2009).
- <sup>29</sup>J. Sue, Y. J. Yan, and S. Mukamel, "Raman excitation profiles of polyatomic molecules in condensed phases. A stochastic theory," *J. Chem. Phys.* **85**, 462–474 (1986).
- <sup>30</sup>S. Mukamel and D. Abramavicius, "Many-body approaches for simulating coherent nonlinear spectroscopies of electronic and vibrational excitons," *Chem. Rev.* **104**, 2073–2098 (2004).
- <sup>31</sup>T. E. Keller and M. H. Rubin, "Theory of two-photon entanglement for spontaneous parametric down-conversion driven by a narrow pump pulse," *Phys. Rev. A* **56**, 1534–1541 (1997).
- <sup>32</sup>F. Schlawin and S. Mukamel, "Matter correlations induced by coupling to quantum light," *Phys. Rev. A* **89**, 013830 (2014).
- <sup>33</sup>S. Lerch and A. Stefanov, "Observing the transition from quantum to classical energy correlations with photon pairs," *Commun. Phys.* **1**, 26 (2018).